Equidimensional modelling of flow and transport processes in fractured porous systems II

Lina Neunhäuserer[a], Susanna Gebauer[b], Steffen Ochs[a], Reinhard Hinkelmann[a], Ralf Kornhuber[b], Rainer Helmig[a]

[a]Institut für Wasserbau, Lehrstuhl für Hydromechanik und Hydrosystemmodellierung, Universität Stuttgart, Germany

[b]Fachbereich Mathematik und Informatik, Institut für Mathematik II, Freie Universität Berlin, Germany

In fractured formations, the vastly different hydraulic properties of fractures and porous matrix lead to a considerable mass exchange between fracture and matrix, strongly affecting the flow and transport conditions in the domain of interest. This plays an important role for many environmental applications, e.g. the design of disposal systems for hazardous waste.

In two papers, we display a new numerical concept describing saturated flow and transport processes in arbitrarily fractured porous media. An equidimensional approach is developed using elements of the same dimension for fracture and matrix discretisation. In *Gebauer et al.* (this issue, part I) we introduced a two–level multigrid method based on a hierarchical decomposition designed to solve equidimensional fracture–matrix–problems. In this paper we will discuss the effect of equidimensionality on the modelling results. Furthermore, the influence of the chosen transport discretisation technique will be shown.

1. INTRODUCTION

The simulation of groundwater flow and solute transport behaviour in fractured subsurface systems is of major importance when investigating the longterm safety of legacies and waste disposal sites, the remediation of contaminant sites, or the safety of aquifers used as drinking–water reservoirs. The complex geometry as well as the vastly different hydraulic properties of fractures and the porous matrix lead to very heterogeneous flow and transport conditions. Numerical concepts employed to describe fractured porous formations have to take these conditions into account.

In both parts of this paper, we will present a discrete model concept for flow and transport processes in fractured porous media. Steady–state flow and an ideal tracer transport are considered. We will introduce an equidimensional approach where fracture and matrix are discretized with elements of the same dimension (fig. 1). Compared to the classical lower–dimensional formulation, the equidimensional approach allows us to obtain flux continuity at the fracture–matrix interface and to determine unique and continuous streamlines.

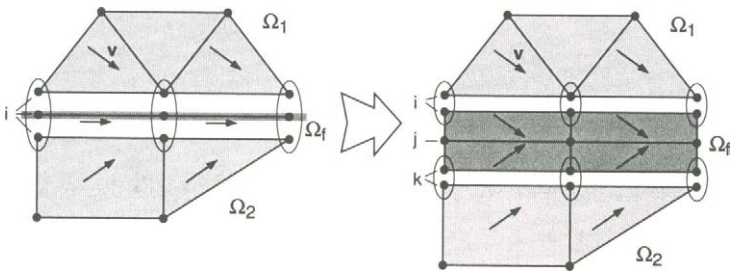

Figure 1. Flux in fracture and matrix depending on the model concept. Left: lowerdimensional formulation. Right: equidimensional formulation.

Part II of this paper will focus on the effects of equidimensional modelling of tracer transport and on transport modelling itself. The transport equation is discretized with a modified box scheme based on a method described by *Noorishad et al.* [9]. It is well suited to take the physical properties of the locally governing process into account and provides a stable solution while reducing artificial dispersion. The applicability of the newly developed model concept will be pointed out by a set of examples. The results of the equidimensional approach will be compared with the results of the lowerdimensional formulation. We will show the influence of the transport discretisation, and we will demonstrate the capability of the two–level multigrid approach introduced in part I.

2. GOVERNING EQUATIONS

In accordance to *Gebauer et al.* (part I) we consider saturated flow in a confined aquifer. Incompressibility of the fluid and nondeformability of the fractured porous medium are assumed. Then the continuity equation in combination with the darcy formula yields the equation for saturated groundwater flow (part I, chapter 2). As from experimental data most often the pressure is obtained instead of the piezometric head, we will use the pressure formulation with $p = \rho g (h - z)$, p is the pressure, ρ the fluid density, g the acceleration due to gravity, h the piezometric head and z the geodetic altitude. Furthermore, we will restrict ourselves to the steady state case:

$$\nabla \cdot (\underline{\underline{K}}_f \nabla p) + \rho g \nabla \cdot (\underline{\underline{K}}_f \nabla z) + \rho g f = 0 \tag{1}$$

$\underline{v}_f$ represents the Darcy velocity, f external sources and sinks and $\underline{\underline{K}}_f$ the hydraulic conductivity tensor.

Knowing the velocity field from equation (1), the advectiv–dispersive transport of an ideal tracer can be described as follows:

$$\frac{\partial c}{\partial t} + \nabla \cdot (\underline{v}_a c) - \nabla \cdot (\underline{\underline{D}} \nabla c) = 0 \tag{2}$$

c stands for the tracer concentration, $\underline{v}_a$ for the interstitial velocity and $\underline{\underline{D}}$ for the effective diffusion tensor defined by *Scheidegger* [10]. From the mathematical point of view, equation (2) inheres a mixed parabolic–hyperbolic character. Dominating dispersion induces a stable parabolic behaviour while strong advection leads to the hyperbolic form which easily excites oscillations.

3. TRANSPORT MODELLING

The transport simulations have been carried out with a conventional and a modified box scheme. These methods have the advantage of being monotonuous and locally mass conservative even on highly unstructured grids [8]. Hence they fulfill an important criterion: they avoid the formation of oscillations which may lead to nonphysical results (e.g., negative concentrations). A BiCG–STAB procedure with a classical multigrid method as a preconditioner has been used to solve the transport discretisation. The transfer of the two–level multigrid approach (part I) to transport problems is object of current research of the authors.

3.1. Box scheme with fully upwinding

The box scheme used here is based on a node centered finite–volume discretisation. Different from cell–centered methods it can be applied to any unstructured grid. Each element is divided into subcontrol volumes. The fluxes perpendicular to the boundaries of the box are determined at the integration points (fig. 2). In the context of a Galerkin–

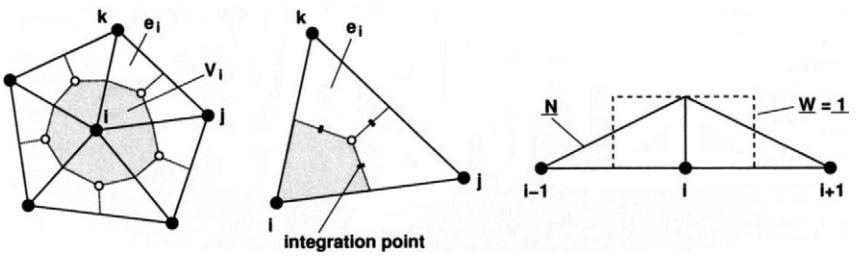

Figure 2. Patch at node i with box V_i, integration points, shape function N and test function W.

finite–element derivation based on weighted residuals

$$\int_\Omega \underline{W} \cdot \epsilon \, dV = 0, \quad \text{with} \quad \epsilon = \mathcal{D}(\tilde{c}) \quad \text{and} \quad \tilde{c} = \underline{N} \cdot \hat{\underline{c}} \tag{3}$$

this corresponds to a formulation with the test function (fig. 2, right)

$$\underline{W} = \begin{cases} 1 \; if \; x \in V_i \\ 0 \; if \; x \notin V_i \end{cases}. \tag{4}$$

The approximation $\tilde{c} = \underline{N} \cdot \hat{\underline{c}}$ is determined for the accumulation term and the dispersion term by means of linear shape functions (fig. 2, right). For the advection term an upstream weighting is carried out (fig. 2, left):

$$c = (1 - \alpha_{ij}) c_{ij} + \alpha_{ij} c_{up} \quad \text{with} \quad \alpha_{ij} = 1 \quad \text{(fully upwinding)} \quad \text{and} \tag{5}$$

$$c_{up} = \begin{cases} c_i \text{ for } \underline{v}_{ij} > 0 \\ c_j \text{ for } \underline{v}_{ij} < 0 \end{cases} \tag{6}$$

c_{ij} is the concentration at the integration point of the subcontrol–volume–interface between nodes i and j, α_{ij} is the belonging upwinding coefficient and $\underline{v}_{ij}$ is the corresponding velocity vector. The method is of first order accuracy for $\alpha = 1$ (fully upwindig) [6,8].

3.2. Box scheme with streamline orientation

Fully upwinding along the element edges provides the system with artificial diffusion which stabilises the solution. As the stabilising diffusion is only needed along the streamlines, we want to minimize the crosswind diffusion. Therefore, we project the upwinding coefficient α_0 along the streamline onto the local normal flux across the interface of the subcontrol volumes of the corresponding nodes (fig. 3, right). Upwinding is still carried

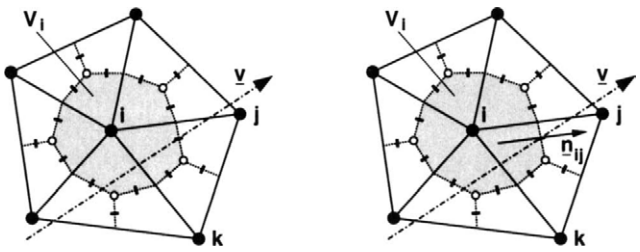

Figure 3. Patch at node i with box V_i. Left: conventional upwinding. Right: projection of α_0 onto n_{ij}.

out along the element edge:

$$c = (1 - \alpha_{ij})c_{ij} + \alpha_{ij}c_i \quad \text{for} \quad \underline{v}_{ij} > 0 \tag{7}$$

Projection of α_0 onto the direction of local flux by means of the normal vector $\underline{n}_{ij}$ yields α_{ij}:

$$\alpha_{ij} = \alpha_0 \frac{\underline{v}_{ij}}{|\underline{v}_{ij}|} \underline{n}_{ij} \tag{8}$$

To optimise the amount of artificial diffusion along the streamline, the determination of α_0 is subjected to the local governing physical processes. An overestimation of α_0 leads to a smearing of the front while an underestimation results in oscillations. The derivation of α_0 is not straightforward for multidimensional problems. The approach outlined here is based on a relationship defined by *Noorishad et al.* [9] and depends on the Courant– and Peclet–number:

$$\alpha_0 = \begin{cases} 0 & \text{for } Cr \cdot Pe \leq 2 \\ Cr - 2/Pe & \text{for } Cr \cdot Pe > 2 \end{cases} \tag{9}$$

Both Courant– and Peclet–number are computed for the n–dimensional space using velocity and dispersion transformed to local coordinates [3]. *Noorishad et al.* [9] use a Crank–Nicholson–Galerkin method. They reach an order of accuracy of two in space and time in areas of dominating dispersion and an order of two in time and of one in space elsewhere. The scheme implemented here is implicit in time. It reaches an order of accuracy of two in time and of one in space for dominating dispersion and an order of one in space and time elsewhere [8].

4. EXAMPLES

The discretisation– and multigrid methods presented in both parts of this paper have been realised within the software system *MUFTE–UG*. *UG* is a software toolbox providing techniques for the numerical solution of partial differential equations [1]. *MUFTE* contains numerous discretisation methods and applications concerning single– and multiphase processes [7,2]. For the domain discretisation the mesh generator *ART* [4,5] in combination with the module *FRACMESH* [8] has been used. *ART* produces triangular meshes of high geometric and combinatoric quality for arbitrarily fractured domains.

4.1. Comparison of lower– and equidimensional approach

The effect of equidimensional modelling on the results of tracer simulation is demonstrated by the following two examples. Domain A is a rather simple one, a homogeneous matrix with an almost verticle fracture (fig. 4, left). Fracture width is $\epsilon = 0.005[m]$. Lower and upper domain boundaries are no–flow–boundaries, on the left and the right hand side dirichlet conditions are imposed with a pressure difference of $\Delta p = 100[Pa]$. The hydraulic conductivities of fracture and matrix differ by three orders of magnitude. Porosity is set to $n_e = 0.3[-]$ for the fracture and $n_e = 0.2[-]$ for the matrix. Molecular diffusion is assumed to be $D_m = 1.0 \cdot 10^{-9}[m^2/s]$, dispersivities are $\alpha_l = \alpha_t = 0.01[m]$ in the matrix and $\alpha_l = 0.1[m]$, $\alpha_t = 0.001[m]$ in the fracture. Tracer enters the domain across the left hand side boundary for 9960[s] with a concentration of $1.0[kg/m^3]$.

Fig. 4 shows domain A with the coarse grid (left) and the pressure distribution which is very similar for the lower– and equidimensional approach at the pictured scale. Nevertheless, the influence of the 2d–fracture on the tracer distribution is obvious when comparing the results in fig. 5.

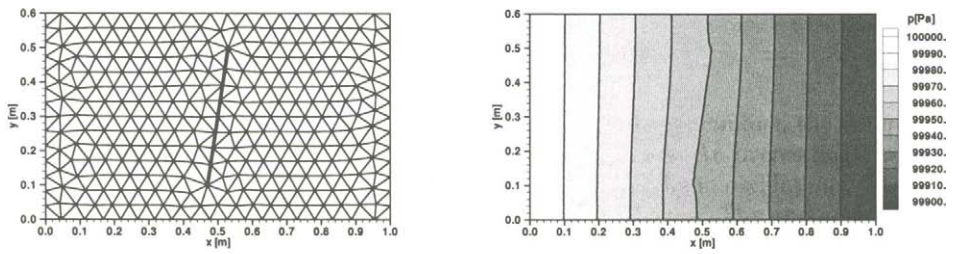

Figure 4. Left: domain A with fracture. Right: pressure distribution.

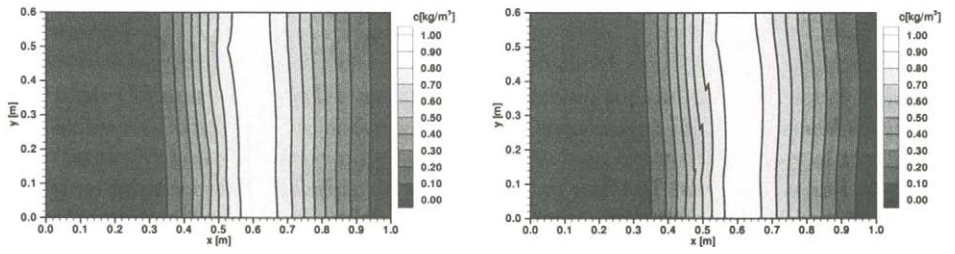

Figure 5. Tracer distribution after 24000[s]. Left: 1d–fracture. Right: 2d–fracture.

Domain B is shown in fig. 6. A fracture network is surrounded by a homogeneous matrix. Boundary conditions and material properties are chosen just as for domain A. The fracture width is set to $\epsilon = 0.01[m]$. Fig. 6 pictures the fractured domain with the pressure distribution and the velocity distribution in the uppermost fracture crossing. The vector plot indicates that the flux is not only moving from the lower left into the lower right fracture of the crossing but that there is a certain amount of mass driven into both the upper fractures of the crossing. This effect cannot be handled with 1d–fractures. Consequently, much more tracer is moving into the dead end fractures (that is, in the upper fractures of the crossing) when using the equidimensional approach (fig. 7).

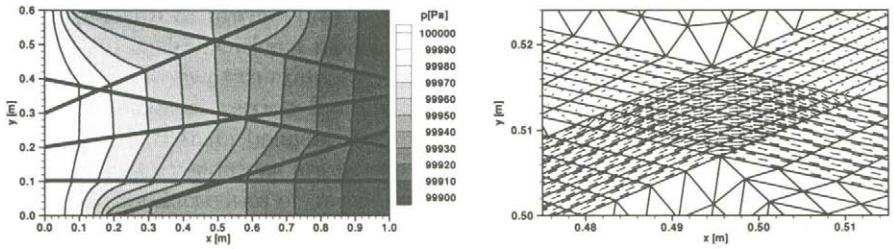

Figure 6. Domain B. Left: fractures, pressure distribution. Right: velocity distribution in upper fracture crossing.

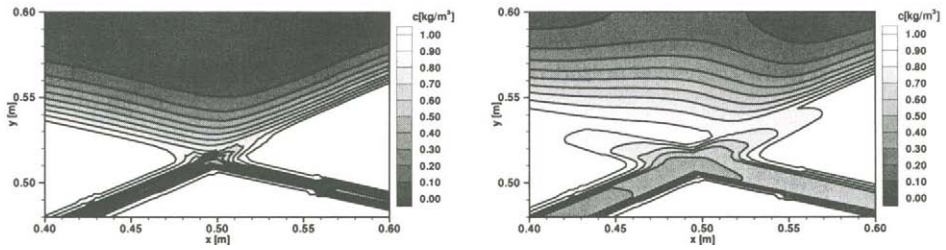

Figure 7. Tracer distribution after 10000[s]. Left: 1d–fractures. Right: 2d–fractures.

4.2. Comparison of upwinding strategies

To demonstrate the influence of the upwinding strategy used for transport modelling, fully upwinding (fu) and streamline orientation (so) are both applied to the example of domain A for different multigrid levels. The fully upwinding scheme has been used up to level 4 (which means, after all, that the coarse grid depicted in fig. 4, left, has been refined four times), the streamline orientation scheme up to level 3. Fig. 8 shows the tracer distribution after 24000[s] for both upwinding strategies applied to level 2. Apparently, with streamline orientation we get a steeper front approximation and a higher peak. This can be expected as most of the domain is matrix, allowing for only small velocities and therefore leaving the box method to second order accuracy. Scanning the tracer profile after 24000[s] and the breakthrough curves from the right hand side domain boundary in fig. 9, it can be seen that the curves not only converge towards a certain value but that using streamline orientation on level 2 leads to a better approximation than fully upwinding on level 4.

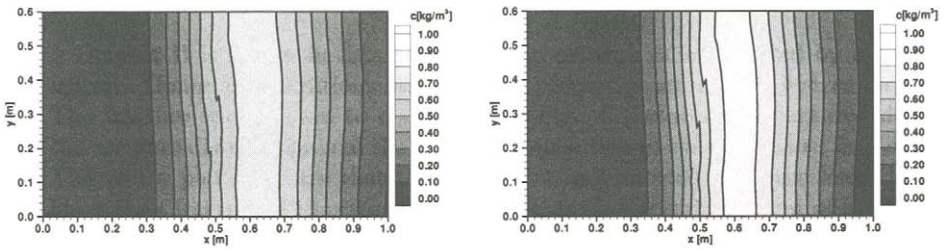

Figure 8. Tracer distribution after 24000[s]. Left: fully upwinding (fu). Right: streamline orientation (so).

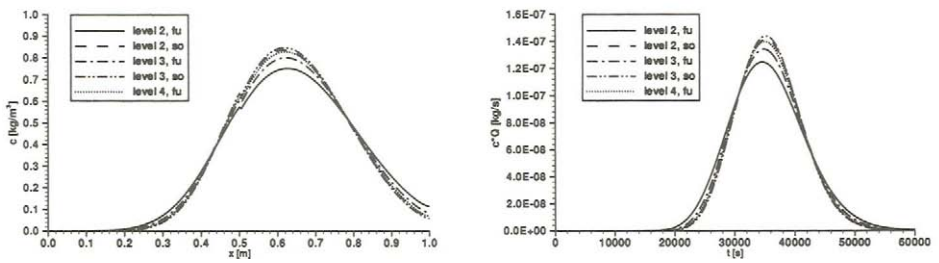

Figure 9. Left: tracer profile at y=0.3[m]. Right: breakthrough curves.

4.3. Conventional multigrid and hierarchical decomposition

Domain B has been chosen to show the capability of the two–level multigrid approach introduced in part I of this paper. Material coefficients and boundary conditions are as before. The fracture width is set to $\epsilon = 1.0 \cdot 10^{-4}[m]$. Fig. 10 represents the pressure distribution computed on grid level 3. It is obvious that the BiCG-STAB using a conventional multigrid method as a preconditioner yields a wrong solution while the problem solved with the two–level multigrid approach remains stable.

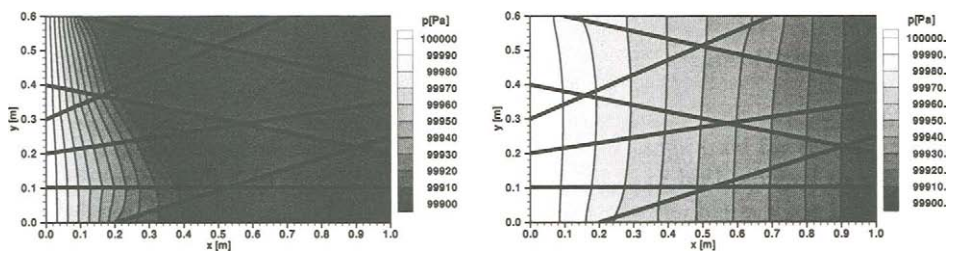

Figure 10. Pressure distribution. Left: conventional multigrid. Right: hierarchical decomposition.

5. CONCLUSIONS

We have introduced a new numerical concept to describe flow and transport processes in fractured porous media. The equidimensional approach enables flux continuity at the fracture–matrix interface, streamline tracing and a better approximation of the velocity field. This is most important as the velocity is a very sensitive parameter to tracer trans-

port. The two–level multigrid method has turned out to provide reliable solutions for decreasing fracture width. Future work will focus on employing h-adaptive refinement, the transfer of the two–level multigrid approach to the transport problem and the development of particle methods for the equidimensional transport simulation.

We thank the Deutsche Forschungsgemeinschaft (DFG) for the funding of this project (see *Neunhäuserer et al.* [8]).

REFERENCES

1. P. Bastian, K. Birken, K. Johannsen, S. Lang, K. Eckstein, N. Neuss, H. Rentz Reichert and C. Wieners. UG – A Flexible Software Toolbox for Solving Partial Differential Equations. Computing and Visualization in Science (1997) 1(1):27–40.
2. T. Breiting, R. Hinkelmann and R. Helmig. Modeling of Hydrosystems with MUFTE–UG: Multiphase Flow and Transport Processes in the Subsurface. In Forth International Conference on Hydroinformatics, Iowa, USA, 2000.
3. O. Cirpka. CONTRACT: A Numerical Tool for Contaminant Transport and Chemical Transformations. Mitteilungen Heft 87, Universität Stuttgart, Institut für Wasserbau, Eigenverlag, 1996.
4. A. Fuchs. Almost Regular Delaunay–Triangulations. International Journal for Numerical Methods in Engineering (1997) 40:4595–4610.
5. A. Fuchs. Optimierte Delaunay–Triangulierungen zur Vernetzung getrimmter NURBS–Körper. PhD–Thesis, Universität Stuttgart, Mathematisches Institut A, Shaker–Verlag, 1999.
6. R. Helmig. Multiphase Flow and Transport Processes in the Subsurface. Springer–Verlag, Heidelberg, 1997.
7. R. Helmig, P. Bastian, H. Class, J. Ewing, R. Hinkelmann, R. Huber, H. Jakobs and H. Sheta. Architecture of the modular program system MUFTE–UG for simulating multiphase flow and transport processes in heterogeneous porous media. In H. Thiergärtner, Hrsg., Mathematische Grundwassermodellierung – unkonventionelle Lösungen und Randbedingungen, Band 2 von Mathematische Geologie. CPress Verlag, Dresden, 1998.
8. L. Neunhäuserer, S. Gebauer, S. Ochs, R. Hinkelmann, R. Kornhuber and R. Helmig. Mehrgittermethoden und adaptive Euler–Lagrange–Verfahren zur Simulation von Strömungs– und Transportvorgängen in Kluftaquifersystemen. Report 01.11.1999–30.10.2001, DFG–Projekte Nr. Ko1806/2–1 und Nr. Hi640/1–1, Universität Stuttgart, Institut für Wasserbau, Lehrstuhl für Hydromechanik und Hydrosystemmodellierung and Freie Universität Berlin, Fachbereich Mathematik und Informatik, Institut für Mathematik II, 2001.
9. J. Noorishad, C.F. Tsang, P. Perrochet and A. Musy. A Perspective on the Numerical Solution of Convection–Dominated Transport Problems: A Price to Pay for the Easy Way Out. Water Resources Research (1992) 28(2):551–561.
10. A.E. Scheidegger. General theory of dispersion in porous media. Journal of Geophysical Research (1961) 66(10):3273–3278.